J. Anat. (1991), **175**, pp. 213–227
With 6 figures
Printed in Great Britain

Subchondral architecture in bones of the canine shoulder

PETER A. SIMKIN, THOMAS F. HESTON, DANIEL J. DOWNEY, RICHARD S. BENEDICT AND HWAN SOO CHOI*

*Division of Rheumatology, Department of Medicine, RG-28 and * Department of Electrical Engineering, FT-10, University of Washington, Seattle, WA 98195, USA*

(*Accepted* 18 *October* 1990)

INTRODUCTION

The normal structure of trabecular bone is not everywhere the same, but varies widely from one site to another. These differences in trabecular design are thought to reflect corresponding differences in mechanical stress. This principle was established over 100 years ago when the crane-like patterns of compressive and tensile trabeculae in the proximal human femur were first so interpreted (Wolff, 1870). As 'Wolff's Law' the stress-dependence of bony architecture is accepted as the basis of the trabecular remodelling that continues throughout life.

To date, however, little emphasis has been placed on quantifying trabecular structure in contrasting regions of normal bone or on refining the correlation of structural findings with varying functional demands. Tools have been developed for assessment of trabecular structure, but these have been applied primarily to the study of metabolic bone disease – usually in biopsy specimens from the iliac crest (Mertz & Schenk, 1970; Parfitt *et al.* 1983; Revell, 1983). Such methods have been useful, for instance, in the diagnosis and management of osteoporosis. Their wider application has been limited, however, by their reliance on 'point counting' techniques (Whitehouse, 1974) or on manual tracing of trabecular outlines on a digitising board (Whitehouse, 1980). These approaches are necessarily limited to small specimens and are, therefore, particularly subject to sampling variation. Furthermore, they rely on human judgment as well as eye–hand coordination and these factors introduce additional sources of error. Thus, studies based on manual methods have introduced useful concepts and have opened substantial opportunities for those interested in anatomical studies of trabecular bone.

In response, a number of investigators have introduced automated methods to capture and analyse two-dimensional images (Albright, Martin & Flohr, 1978; Fazzalari, Darracott & Vernon-Roberts, 1983; Beigbeder *et al.* 1988). This approach is particularly well-suited to analysis of bone structure, since the computer must only distinguish between bone and adjacent soft tissues. If appropriate measures are taken to ensure that an image is truly two-dimensional, and is thus free of the transmission artefacts inherent in thick sections, automated techniques should permit accurate quantification of structure at any skeletal site.

Our desire to quantify patterns of trabecular bone grew out of an established interest in consistent structural and functional differences between the convex and concave members of normal 'ball and socket' joints (Simkin, Graney & Fiechtner, 1980). Previous work led us to expect a stiff concave structure of simple design opposed to a flexible convex component supported by a more complex trabecular framework (Simkin, Pickerell & Wallis, 1985; Simkin, Houglum & Pickerell, 1985;

Downey, Simkin & Taggart, 1988). For the present investigation, we developed an automated system employing digitised images to evaluate subchondral plate thickness as well as underlying trabecular bone volume, mean trabecular density, mean trabecular thickness, mean trabecular separation, surface to volume ratio and surface density of trabecular bone. We applied this methodology to evaluate the structure of juxta-articular, subchondral bone in the canine humerus and scapula.

METHODS

Section preparation

Opposing bones of both canine shoulder joints were obtained from nine dogs used in unrelated studies of cardiopulmonary physiology. Adjacent soft tissues were removed by dissection and cleaned specimens were then hard-frozen in liquid nitrogen prior to being cut into coronal and transverse slabs, 2–3 mm thick, with an 'Exacto' razor saw (Model 240). Additional liquid nitrogen was used as necessary to keep the marrow frozen and thus prevent trabecular breakage during the cutting process (method modified from Whitehouse, Dyson & Jackson, 1971). After thawing, the sections were cleaned by irrigation, immersed in a bath of 50% ethylene glycol for 20 minutes at 70 °C and rinsed twice in distilled water. Final treatment in 3% hydrogen peroxide for approximately two hours removed any remaining soft tissue and softened the articular cartilage for easy manual removal.

In each dog, transverse sections were taken from one shoulder together with coronal sections through the bones of the contralateral side. Thus, sections at right angles to each other were prepared from the two sets of shoulder bones obtained from each dog.

After air-drying, all the specimens were embedded in white polystyrene. They were first placed at room temperature in uncatalysed Bioplastic (Wards Bioscience) containing styrene monomer, in a ratio of 4–1, and white fibreglass resin pigment. Immersed specimens were maintained under reduced pressure (250 mmHg) for 12 hours to facilitate removal of air bubbles and were then transferred to individual shallow containers of Bioplastic solution with added catalyst. After curing at atmospheric pressure and room temperature for 24 hours, specimens were baked at 60 °C for 4–6 hours to accomplish final hardening.

The hardened specimens were ground on a revolving disc with 80 grit silicon carbide to expose the bone surface, smoothed with 180 grit and polished on a 45 μm diamond disc. Specimens with surface defects due to air bubbles were reimpregnated and resmoothed. All specimens were then stained by placing them face-down on filter paper soaked with 1·5 M silver nitrate solution and then exposing the stained surface to daylight. The finished specimens resembled scrimshaw with a pattern of black trabecular bone against a background of white polystyrene (Fig. 1).

Imaging

A Leitz Wetzlar 35 mm camera, mounted on a Wild Heerbrug MB stereomicroscope with an MPS 11 shutterpiece and constant lighting, was used to photograph the weight-bearing areas of each specimen using Kodak Technical Pan film. Each photograph included a millimetre ruler as a gnomon. The prints were enlarged 27 times and areas of bone, including the osteochondral junction, were selected for analysis by a CAT 1600/11 image processing system (Digital Graphics, Palo Alto, CA) hosted by a MC68010-based microcomputer. A 2 mm by 10 mm window, normal to the articular surface, was then selected for further analysis. The digitised image consisted of a simple grid containing 400 rows, each of which was 100 pixels across.

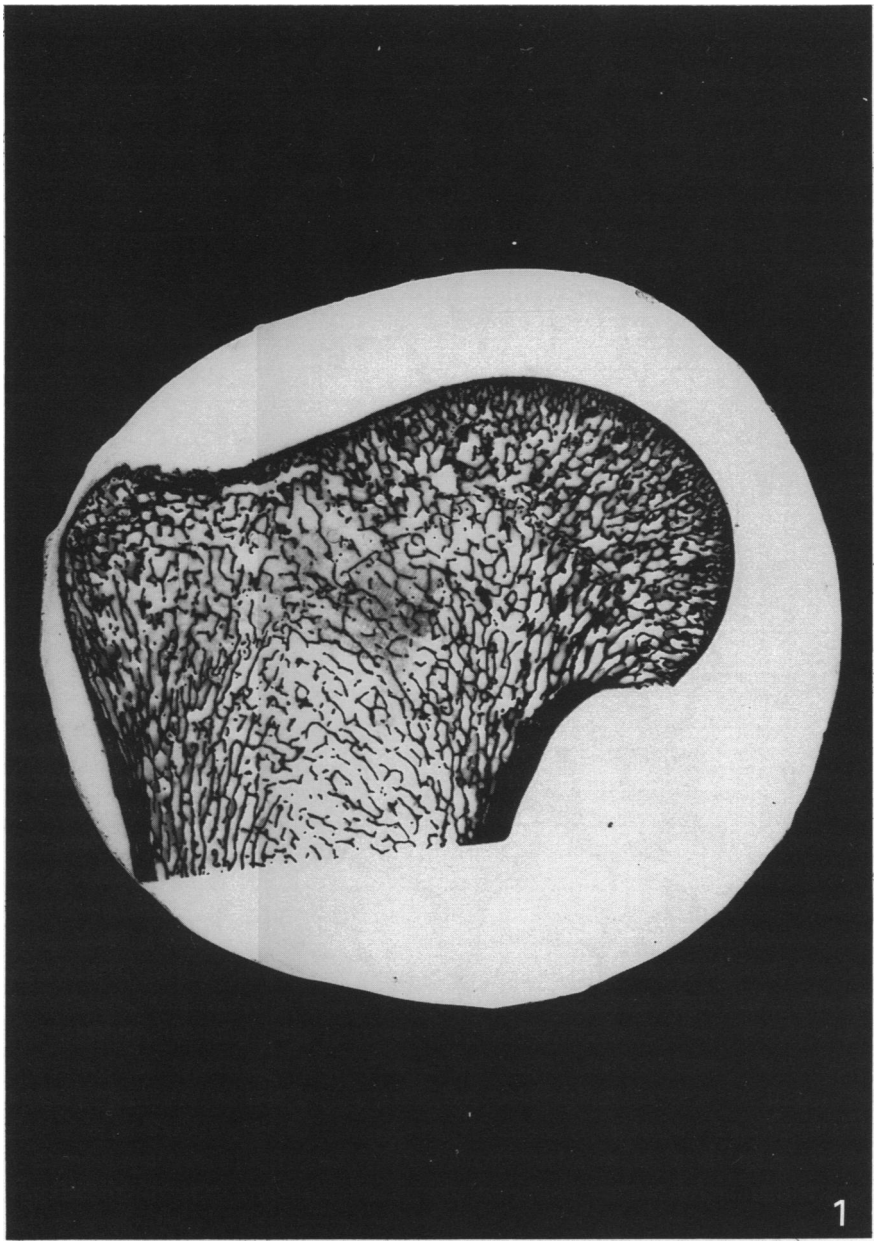

Fig. 1. Coronal section of a proximal canine humerus. After soft tissue removal, slab section was embedded in a disc of white polystyrene and stained with silver stain. The resulting preparation of black trabecular bone against white plastic resembles scrimshaw.

Careful attention to scale ensured that each pixel measured 20 μm across and 25 μm in depth.

Each of the 40 000 pixels per image was initially recorded in one of 256 levels of grey. Appropriate thresholding was then employed to reduce this information to a binary system, where each pixel was considered either black (bone) or white (marrow space). For this purpose, setting a constant grey level of 85 provided the most satisfactory

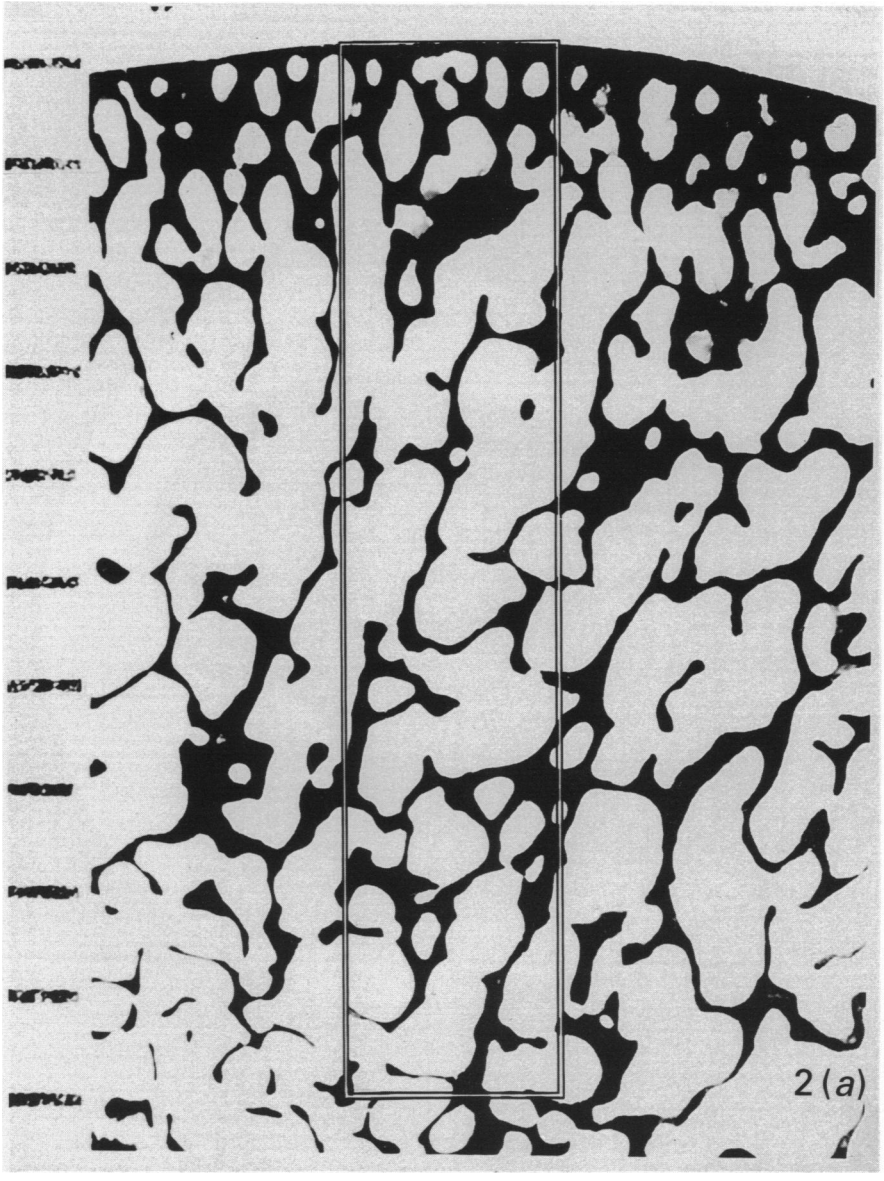

Fig. 2 (*a–b*). Subchondral bone of canine humerus (*a*) and scapula (*b*). 'Scrimshaw' preparations have been photographed and enlarged with millimetre rules along the left-hand margins. Rectangular overlays indicate representative 2 mm × 10 mm 'windows' that were digitised for analysis as 100 × 400 pixel images.

demarcation point, where 1 is white and 256 is black. This cut-off point was used for all of the images.

The long axis of the bone windows was normal to a line tangential to the osteochondral junction of each specimen (Fig. 2). In the transverse sections, single sites (Fig. 3) were located in the centre of the articular surfaces of the humerus (*C*) and the scapula (*F*). Two sites were analysed in the coronal section of the humerus. One of these (*A*) was based at the area of maximal convexity in the normal impact area of the humeral head, while the second site (*B*) was placed further posteriorly in order to

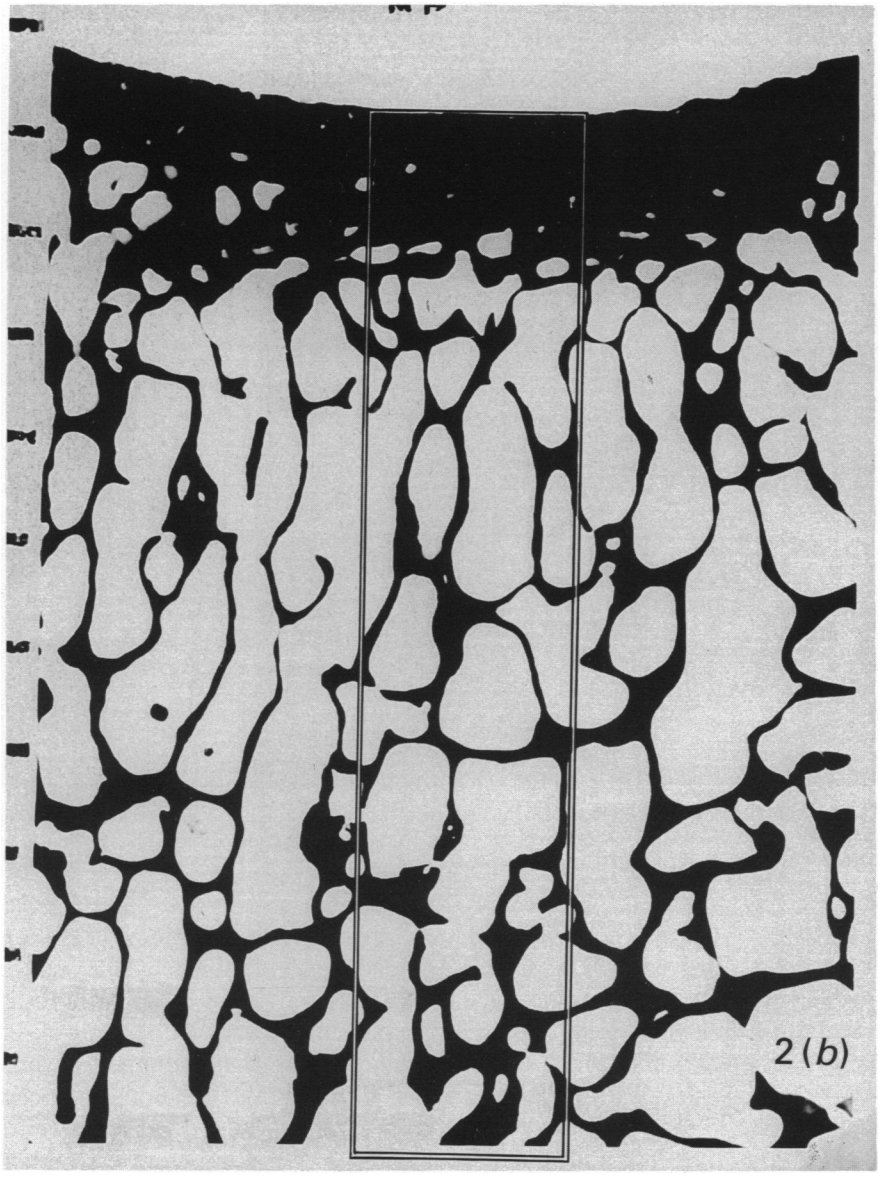

eliminate or minimise overlap as these fields converged with increasing subchondral depth. In the coronal section of the scapula, two adjacent 2 mm sites (*D* and *E*) were also employed, which diverged with increasing subchondral depth.

Structural variables

In every case, Row 1 was determined as the first row having a density of 50% or more, i.e. at least 50 of its 100 pixels were black. This convention was necessary because of the natural convexity or concavity of the humeral and scapular surfaces. This percentage rose in subsequent rows and usually reached 100% by Row 3. The subchondral plate thickness (SCPT) was defined as the product of the height of each pixel row (25 μm) and the number of the last row having a density of at least 95%.

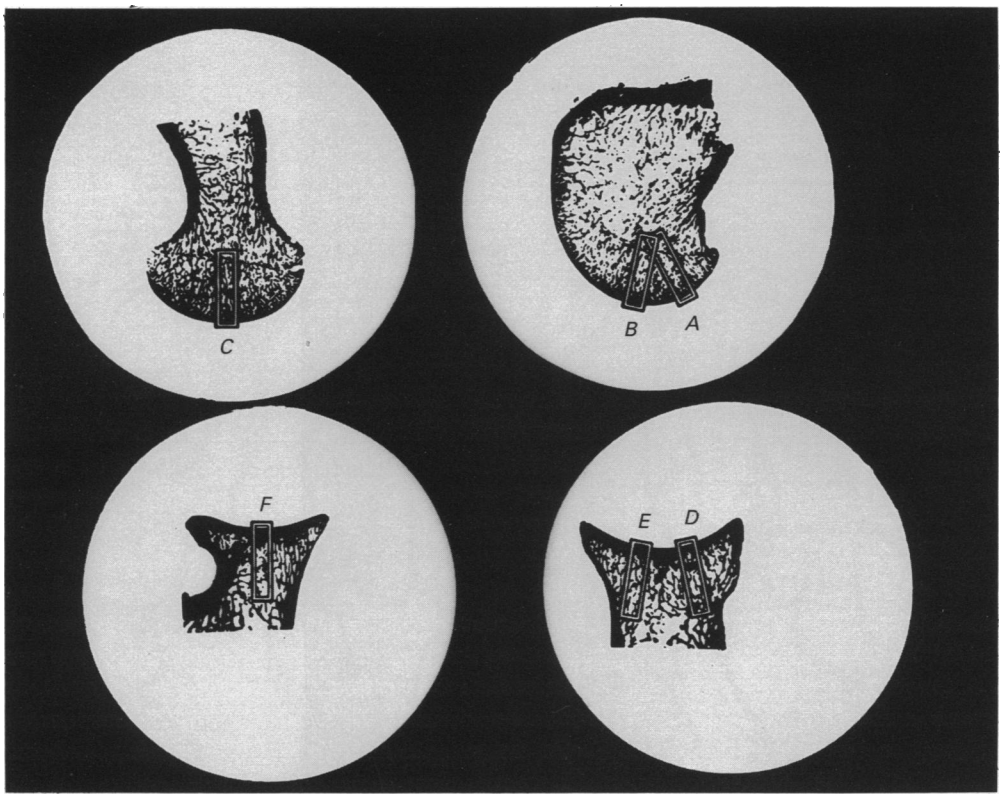

Fig. 3. Coronal and transverse sections through left and right shoulder bones of a normal dog. Rectangular overlays (*A–F*) depict sites chosen for quantitative evaluation of subchondral trabecular structure.

Each of Rows 1–400 was analysed to determine its total bone volume (TBV) and its mean trabecular density (MTD). TBV is the density determined by the number of black pixels out of the 100 in each row, and expressed as a whole number in the range from 0 to 100. It may also be considered as the percentage of bone per unit of surface area. MTD is the number of trabeculae (which equals the number of marrow chambers) per mm of width. It was determined by counting the number of marrow-to-bone and bone-to-marrow transitions in each 2 mm row and dividing by four. It is expressed in mm^{-1}.

From the basic observation of TBV and MTD and the known dimensions of each pixel, four additional variables were determined: mean trabecular thickness (MTT) is the average thickness of trabeculae crossed by each row. It was determined by the formula:

$$\text{MTT} = \frac{\text{TBV} \times 20\ \mu\text{m}}{\text{MTD} \times 2\ \text{mm}}$$

and is expressed in μm. The 20 μm term in this equation is the width of each pixel.

Mean trabecular separation (MTS) is a comparable entity describing the average marrow chamber width or space between trabeculae. It was determined by:

$$\text{MTS} = \frac{(100 - \text{TBV}) \times 20\ \mu\text{m}}{\text{MTD} \times 2\ \text{mm}}$$

and is also expressed in μm.

The bone surface density (S_v) is the surface to volume ratio or the area per unit of total tissue volume. It was calculated for each row by:

$$S_v = \frac{4 \times \text{MTD} \times 25\ \mu\text{m}}{25\ \mu\text{m} \times 2\ \text{mm}}$$

which reduces to $2 \times \text{MTD}$.

The specific surface S/V is the trabecular surface area per unit of trabecular volume (mineralised tissue) and is simply obtained from the formula:

$$S/V = \frac{100 \times \text{Sv}}{\text{TBV}}.$$

Both surface density (S_v) and specific surface (S/V) are expressed in (mm^2/mm^3) in accord with the principle of deLesse.This convention, which assumes that patterns observed in two-dimensional sections will be similar in the third, unexamined dimension, has been verified in studies of human iliac trabecular bone (Schwartz & Recker, 1981).

Unless otherwise noted, statistical comparisons were by the two-tailed, paired *t* test. All mean values are given $\pm$ one standard error of the mean.

RESULTS

Coronal sections

As noted, coronal section windows from the humerus were taken from somewhat different locations. Window A was anterior in a site felt to be that loaded on impact during running, while Window B was posterior to A in an area more likely to be loaded during static weight bearing (Fig. 3). There were modest, but significant, differences between the structure of these sites: the density (TBV) was greater, the trabeculae (MTT) were thicker and the chamber size (MTS) smaller in A than B. These differences were small, however, and they will not be presented here.

There were no significant differences between windows D and E in the coronal section of the scapula.

Transverse sections

The plane used in cutting the transverse humeral sections was perpendicular to the articular surface and slightly posterior to Window A. In comparing transverse and coronal features, the single transverse window, C, was therefore compared to the mean of Windows A and B. Similarly, the mean of coronal scapular Windows D and E was compared to the single transverse Window F.

Both in the humerus and the scapula, these comparisons revealed no essential differences in trabecular structure between sections cut perpendicular to each other. Their structure thus appeared to be isotropic.

Radius of curvature

The radius of surface curvature was calculated by simple Pythagorean geometry. Accurate analyses required a flawless surface and pixel rows 1 and 3 had to have density (TBV) values greater than 50 and less than 95. When those conditions were not met, the calculation gave unreasonable radii that were either too large or too small. Because these problems gave our results a non-gaussian distribution with unacceptable outliers, we chose to report the median values from all samples. In the humerus, the median radius of curvature was 6·34 cm, while in the scapula, it was 6·79 cm.

Scapula versus humerus

In both bones of the shoulder joint, the trabecular architecture can be considered as a subchondral plate supported by a transitional region above an underlying deep zone of relatively constant structure. Of these, the subchondral plate and the constant zone are best suited for quantitative analysis. For that analysis, all three windows were used to characterise the structure of each bone. In order to weigh the data from left and right shoulders equally, the data from each pixel row in the single transverse section were doubled, then added to those from the same depth in the two coronal windows, and the total was then divided by four to obtain mean values for each experimental variable.

In practice, the subchondral plate is not a completely solid structure, but is one that contains occasional vascular channels and rare, small marrow spaces. It thus is not appropriate to require a TBV of 100% in defining this structural feature. Instead, we characterised the lower border of the subchondral plate as that pixel row where TBV fell below 95%. So defined, the mean subchondral plate thickness of the scapula was 764 ± 24 (S.E.M.) μm, whereas that of the opposing humerus was 147 ± 7 μm ($P < 0{\cdot}001$). For each dog, this difference between the concave and convex joint members was also evaluated by the ratio of scapular to humeral subchondral plate thicknesses. The geometric mean of these ratios was 5·6.

In the transitional region beneath the subchondral plate, the width of the marrow spaces progressively increased until a deeper, stable zone was reached. This transition had invariably been completed by a depth of 5 mm. We therefore used the mean of all data between 5 and 10 mm (pixel Rows 201 and 400) to quantify and compare the trabecular structure of each distal scapula and proximal humerus. Of course, data for individual rows within this range varied above and below the mean. To determine the depth of the transitional zone, we measured the distance from the bottom of the subchondral plate to the point where the density first fell below the mean and remained there for five or more consecutive pixel rows. So defined, the transitional region in the humerus, 3210 ± 340 μm, was greater than that in the scapula, 2650 ± 210 μm. Thus, the thick subchondral plate of the scapula is supported by a trabecular framework that rapidly adopts a consistent deep structure. In contrast, the thin subchondral plate of the humerus overlies a wider transitional zone of progressively increasing chamber size before reaching the stable structural pattern of deeper bone.

Mean data from the 5 to 10 mm deep zone were evaluated in a number of ways. As already described, the data from each dog represented the average of two windows from the left (coronally sectioned) and one window from the right (transversely sectioned) shoulder bones of the same animal. The deep zone of each window contained 200 rows of 100 pixels, thus making a total of 20000 pixels. The trabecular bone volume simply represented the density or the percentage of the pixels that lay over bone. The mean trabecular bone volume of the humerus was $29{\cdot}3 \pm 2{\cdot}2$%, as opposed to a lower value in the scapula of $22{\cdot}7 \pm 0{\cdot}9$% ($P < 0{\cdot}05$).

Mean trabecular distance is simply the number of trabeculae per mm. It was determined by counting the transitions between bone and marrow space in each 2 mm pixel row, and dividing by 4. This value in the humerus, $1{\cdot}34 \pm 0{\cdot}04$ mm^{-1}, was significantly greater than that in the scapula, $1{\cdot}00 \pm 0{\cdot}04$ mm^{-1}, $P < 0{\cdot}01$.

Mean trabecular thickness, the third trabecular variable, is derived from the total bone volume and the mean trabecular density by multiplying the pixel width (20 μm), times TBV, divided by MTD. This formula actually overestimates the trabecular width because it sees horizontal trabeculae above and below marrow spaces

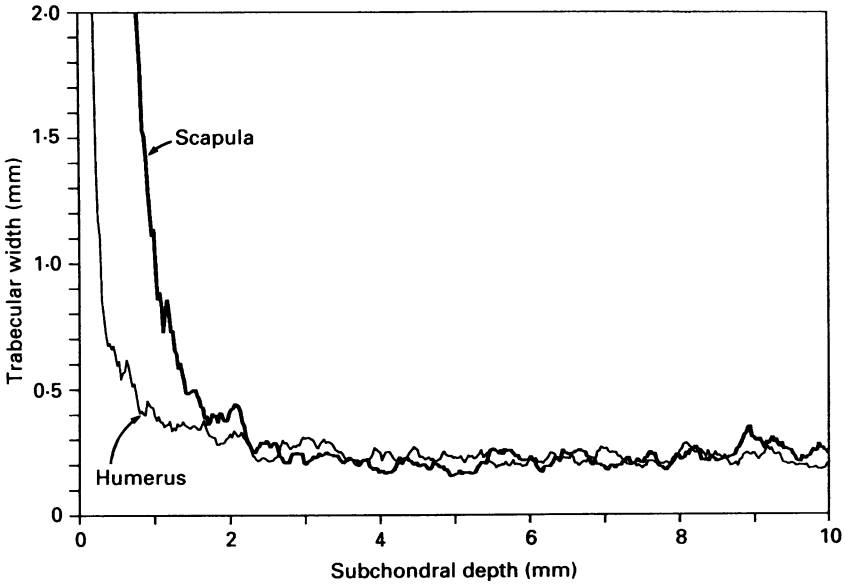

Fig. 4. Mean trabecular thickness as a function of subchondral depth in the canine humerus and scapula. The subchondral plate is significantly thicker in the scapula than in the humerus. At deeper levels, the trabecular width does not differ between the humerus and the scapula.

tangentially as single wide trabeculae, and it similarly overestimates the width of all trabeculae crossed by pixel paths at anything other than a right angle. Without more detailed information on trabecular orientation in either bone, however, we feel that this first approximation remains the most appropriate form of analysis for this comparison of humeral and scapular structure.

Row by row, the progression of this variable from the subchondral plate through the transitional region to the relatively stable deep zone is shown in Figure 4. Within the deep zone, the mean trabecular thickness in the humerus, 217 ± 11 μm, did not differ from that of the scapula, 230 ± 9 μm.

Mean trabecular separation was evaluated by similar methods. Here, the focus changed to the pixels overlying marrow cavities. The formula used was pixel width (20 μm) times 100 minus the TBV divided by MTD. This approach yields the average length of all pixel rows across marrow spaces and therefore provided values lower than would the pixel path at the widest point of each space. These data revealed that trabecular separation is essentially nonexistent in the subchondral plate, increases progressively through the transitional region, and then stabilises in the deeper zone between 5 and 10 mm (Fig. 5). In that region, the mean trabecular separation in the scapula, 791 ± 40 μm, was significantly greater than that at the same depth in the humeral head, 538 ± 33, $P < 0{\cdot}05$.

The mean trabecular density was also used to calculate the 'surface to volume ratio', S_v. This value is an expression of the length of trabecular margin per unit of bone surface area. To obtain this value, MTD was multiplied by two to include both sides of each trabecula and by the pixel height, 25 μm in each row. These values were summed for all of the 200 rows between 5 and 10 mm, and the total was divided by the deep surface area assessed in each window, 10 mm^2 or 0·01 cm^2. The principle of deLesse is regularly applied to such data to extend the interpretation into the third dimension and express the values in mm^2/mm^3. The essential isotropy demonstrated in our comparison of transverse and coronal sections appears to confirm the validity

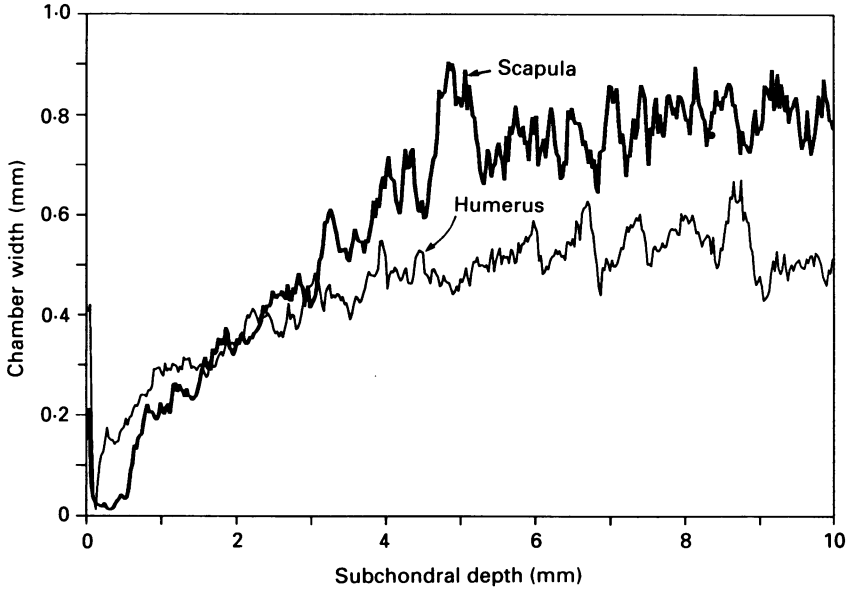

Fig. 5. Mean trabecular separation as a function of subchondral depth in the canine humerus and scapula. Intraosseous chambers are small in both bones within the immediate subchondral region. In the deeper zone between 5 and 10 mm, intraosseous chambers are significantly wider in the scapula than in the humerus.

of this approach for the canine scapula and humerus. In the absence of specific information on trabecular orientation, the data were not corrected for obliquity and therefore they underestimate the true total length of trabecular margins. The surface to volume ratio of the humerus, $2{\cdot}67 \pm 0{\cdot}08$ mm^2/mm^3, was significantly greater than that of the scapula, $1{\cdot}99 \pm 0{\cdot}08$ mm^2/mm^3 ($P < 0{\cdot}01$).

Finally, the surface density was also evaluated. This entity reflects the surface per unit of bone mass. It was obtained by dividing the surface to volume ratio by the trabecular bone volume (%). The value obtained for the humerus, $9{\cdot}5 \pm 0{\cdot}6$ mm^2/mm^3, did not differ significantly from that for the scapula, $8{\cdot}8 \pm 0{\cdot}03$ mm^2/mm^3. Structural variables for each animal are listed in Table 1.

Structural correlations

In order to evaluate interrelationships among the structural variables, we constructed a simple grid listing Pearson correlation coefficients for each possible pair of variables within our study population of 9 animals (Table 2). In both the humerus and the scapula, there were weakly significant ($P < 0{\cdot}05$) positive correlations between subchondral plate thickness and both the total bone volume and the mean trabecular thickness in the underlying matrix of spongy bone. Furthermore, there were negative correlations between SCPT and the surface to volume ratio (S/V) in both bones, but only that in the scapula reached significance ($r = 0{\cdot}81$, $P < 0{\cdot}05$).

Among the variables determined in the deep, 5–10 mm zone, there was a higher intercorrelation in the humerus than in the scapula. This structural uniformity is reflected by a median value of 0·925 for all correlations in the 5–10 mm zone of the humerus, in contrast to a median of 0·505 in the corresponding region of the scapula. Thus, there was much more consistent organisation of bone structure within the humerus than was present in the scapula.

Table 1. *Structural features of scapula and humerus in nine adult dogs*

Dog no.	SCPT	TBV	MTD	MTT	MTS	S_v	S/V
			Scapula				
1	0·825	21·4	0·775	276	1014	1·55	7·24
2	1·100	25·2	1·020	247	733	2·04	8·09
3	0·525	22·8	1·166	195	662	2·33	10·24
4	1·100	27·9	1·121	249	643	2·24	8·04
5	0·650	20·3	0·949	213	841	1·90	9·37
6	0·750	23·0	1·034	223	744	2·07	8·97
7	0·500	18·0	0·898	200	913	1·80	9·99
8	0·875	22·5	0·880	256	880	1·76	7·81
9	0·550	23·4	1·111	210	690	2·22	9·51
			Humerus				
1	0·275	37·5	1·42	265	441	2·84	7·55
2	0·175	34·0	1·41	241	468	2·82	8·32
3	0·175	30·7	1·44	213	482	2·88	9·38
4	0·175	35·6	1·54	231	418	3·08	8·65
5	0·125	34·0	1·35	251	487	2·71	7·98
6	0·175	27·4	1·24	222	587	2·47	9·00
7	0·050	24·1	1·29	187	586	2·59	10·72
8	0·075	22·9	1·21	189	637	2·42	10·56
9	0·100	17·0	1·13	151	737	2·25	13·27
Mean scapula	0·764	22·7	0·995	230	791	1·99	8·81
S.E.M.	0·073	0·9	0·041	8	40	0·08	0·33
Mean humerus	0·147	29·3	1·337	216	538	2·67	9·49
S.E.M.	0·021	2·2	0·041	11	33	0·08	0·56
P	< 0·001	< 0·01	< 0·001	NS	< 0·01	< 0·001	NS

TBV, total bone volume; MTD, mean trabecular distance; MTT, mean trabecular thickness; MTS, mean trabecular separation; S/V, specific surface; SCPT, subchondral plate thickness; S_v, surface to volume ratio.

Table 2. *Correlation matrix of structural variables in humeral and scapular specimens. Values are Pearson correlation coefficients, r*

		TBV	MTD	MTT	MTS	S/V	SCPT	
Scapula	TBV	—	0·88++	0·96+++	−0·97+++	−0·95+++	0·75+	Humerus
	MTD	0·58	—	0·72+	−0·96+++	−0·75+	0·58	
	MTT	0·38	−0·52	—	−0·88++	−0·98+++	0·75+	
	MTS	−0·70+	−0·98+++	0·39	—	0·90++	−0·66	
	S/V	−0·42	0·49	−0·99+++	−0·35	—	−0·69+	
	SCPT	0·74+	−0·05	0·78+	−0·13	−0·81+	—	

Probabilities of significant relationships by 2-tailed *t* test, uncorrected for the number of correlations, are: + = $P < 0·05$, ++ = $P < 0·01$, and +++ = $P < 0·001$.

Values above and to the right of the diagonal spaces are from the humerus. Those below and to the left are from the scapula.

The most striking aspect of the correlation grid, however, is that certain morphometric indices correlated positively in one bone but were negatively related in the other. For instance, the relationship between mean trabecular separation (MTS) and mean trabecular thickness (MTT) was negative in the humerus (−0·88) but positive in the scapula (0·39) (Fig. 6). Conversely, MTS correlated positively with S/V, the surface to volume ratio, in the humerus (0·90), but this relationship was negative in the scapula (−0·35). Comparable contrasts were present between MTT and the mean trabecular density (MTD) (0·72 in the humerus and −0·52 in the scapula) and between MTD and S/V (−0·75 in the humerus and 0·49 in the scapula). By F-test,

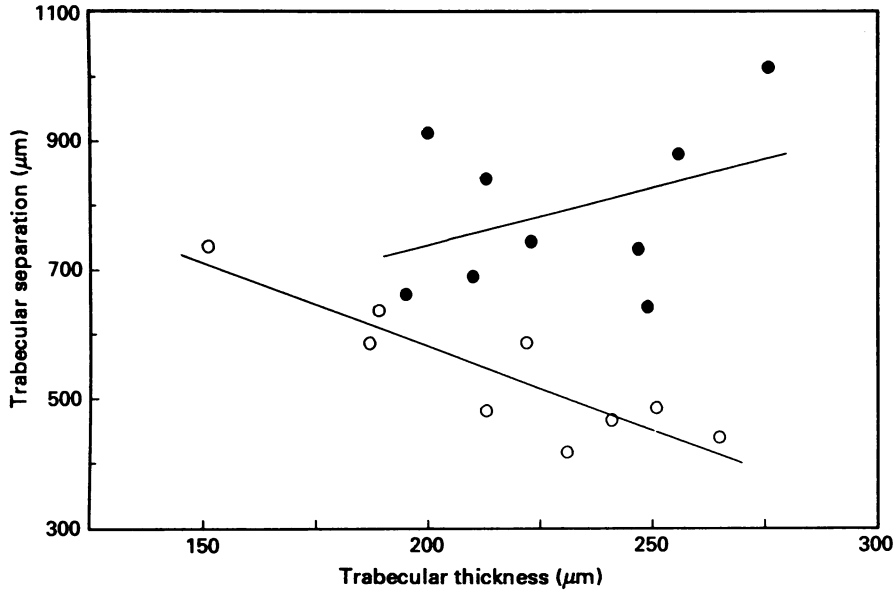

Fig. 6. The relationship between mean trabecular separation and mean trabecular thickness in trabecular bone 5–10 mm beneath the articular cartilage in the scapulae (closed circles) and humeri (open circles) of nine adult dogs. Trabecular separation is greater in the scapula than in the humerus, but trabecular thickness does not differ. The relationship between these variables is strongly negative in the humerus ($r = -0{\cdot}88$) and is weakly positive in the scapula ($r = 0{\cdot}39$).

all of these differences are statistically significant. The overall pattern appears to be one in which increased trabecular spacing leads to conservation of surface area at the expense of trabecular thickness in the humerus. The converse relationships pertain within the scapula, where increased trabecular spacing leads to conservation of trabecular thickness at the expense of surface area.

DISCUSSION

This study of canine shoulder bones quantifies and extends the convex-concave structural differences first evaluated in microradiographs of normal human joints (Simkin *et al.* 1980). The most obvious of these differences is in the subchondral plate. In the average dog, this structure is 5·6 times thicker in the glenoid fossa than it is in the opposing humeral head. Less obvious, but of comparable statistical significance, are the structural differences in the underlying bone. In the humerus, chamber size gradually increases and trabecular thickness thins throughout a broader transitional zone than that found within the scapula. Beyond 5 mm beneath the cartilage, the structure stabilises with trabeculae of comparable thickness in both bones, but significantly smaller chambers and more consistent organisation in the humerus than in the scapula. A higher level of organisation in the convex side of weight-bearing joints has also been observed in the human knee joint (Behrens, Walker & Shoji, 1974).

These structural findings are consistent with the functional differences that have already been established between the canine humerus and scapula. Under load, the humerus was six times more compliant than the scapula (Simkin *et al.* 1985). We believe this difference primarily reflects the greater thickness of the scapular subchondral plate. This dense structure is firmly anchored to cortical bone at the

glenoid margins and seems well adapted to resist displacement under load. Basic architectural principles explain the logic of a stiff concave subchondral plate. Loading of convex surfaces is like that upon a Roman arch. Since the stress compacts the surface elements, the arch can flex and still remain strong. In contrast, loading stress in a concave arch induces tensile stresses tangential to the surface. If this surface flexes, its constituent parts will move away from each other and the entire system will fail. Thus, it is not surprising that the subchondral structure of the scapula is significantly different from that of the humeral head.

The mean subchondral plate of the canine scapula, 792 μm, remains much thinner than that measured directly on microradiographs of concave human joints. For instance, the mean subchondral plate of the human scapula was measured as $2{\cdot}3 \pm 0{\cdot}7$ mm and that of the acetabulum as $2{\cdot}6 \pm 0{\cdot}7$ mm (Simkin *et al.* 1980). In part, this interspecies difference may reflect the greater precision of the methods used in the present study. In part, as well, the difference could reflect the larger size of the human body. We believe, however, that there is a more important reason why concave subchondral plates of human joints will be thicker than those of corresponding canine articulations. Wolff's law implies that bone formation will vary in response to differing degrees of stress. Under constant pressure (P), the tensile stress (T) in a spherical wall will increase in direct proportion to increases in radius (r). This well-known principle of $T = Pr$ is known as the law of LaPlace. Logically, it leads us to expect that larger animals will require substantially thicker subchondral plates in order to prevent failure of subchondral joint surfaces under impact loads. Preliminary observations of hip and shoulder bones from large quadrupeds are consistent with this interpretation. Similarly, one would expect, within any one species, that concave subchondral plates of different joints would vary in proportion to their radius of curvature as well as their loading pressures. This may well explain why the glenoid fossa, for instance, appears to be much better supported than the distal interphalangeal joints of human beings.

The other established difference between the canine humerus and scapula lies in the resistance to saline infused through a needle whose tip lies 5 mm beneath the surface of articular cartilage (Simkin *et al.* 1985). In this work, the hydraulic resistance was approximately ten times greater in the humerus than it was in the scapula. That difference presumably reflects a much reduced connectivity between adjoining marrow chambers. We were not able to quantify connectivity, a third-dimensional property, in the present two-dimensional work. It seems reasonable to suspect, however, that the significantly smaller marrow spaces of the humerus communicate through narrower channels than do the more open chambers of the scapula.

The more flexible humeral surface implies that impact loading will displace fluid within underlying trabecular spaces. That fluid pulses or flow, will then encounter greater resistance within the smaller chambers and connections of this convex bone. These observations necessarily imply that articular loading will raise intraosseous pressures to a greater degree in convex joint members than it will within their concave mates. This, in fact, was found to be the case in recent studies of human hips where loads within the physiological range induced pressures 3·6 times higher within the femoral head than they did above the opposing acetabulum (Downey *et al.* 1988). These observations raise again the old question of possible hydraulic distribution of loading energy under impact load (Frost, 1964). They focus this question, however, on the convex member of 'ball and socket' joints. The morphometric correlations in this study are consistent with an interpretation whereby hydraulic stresses lead to increased trabecular surface in the humerus while mechanical stresses lead to increased trabecular thickness in the scapula. Further studies will be needed to confirm this

possible role of load-induced pressure pulses in the mechanics of subchondral trabecular bone and in the pathogenesis of lesions peculiar to these sites (Simkin & Downey, 1987).

SUMMARY

The distal scapula and proximal humerus from each shoulder of nine adult dogs were slab-sectioned, cleaned of soft tissues, embedded in white plastic and stained black with a silver stain. These preparations were then photographed for automated, digital, morphometric analysis of subchondral bone structure. Comparison of transverse and coronal sections through the left and right shoulders demonstrated essential isometry of trabecular patterns within each bone. Comparison of the scapula and humerus revealed significant differences in bony architecture. The subchondral plate was an average of 5·6 times thicker under the glenoid fossa than in the opposing humeral head. Deeper trabecular structure also differed with the trabecular bone volume (density) in the humerus being greater than that in the scapula. This difference reflects a greater trabecular density in the humerus with comparable trabecular thickness in both bones. These structural differences are consistent with previous functional studies of the same two bones that revealed greater mechanical stiffness beneath the glenoid fossa and greater hydraulic resistance within the humeral head.

Supported in part by NIH Grant AM32811 and by Arthritis Research Center and Washington Chapter grants from the Arthritis Foundation.

REFERENCES

ALBRIGHT, J., MARTIN, R. & FLOHR, R. (1978). Automatic image analysis of the bone biopsy: Variations in rib architecture. *Microscope* **26**, 15–33.

BEHRENS, J. C., WALKER, P. S. & SHOJI, H. (1974). Variations in strength and structure of cancellous bone at the knee. *Journal of Biomechanics* **7**, 201–207.

BEIGBEDER, M., CHAPPARD, D., ALEXANDRE, C., VICO, L., PALLE, S. & RIFFAT, G. (1988). Improved algorithms for automatic bone histomorphometry on a numerized image analysis system. *Journal of Microscopy* **150**, 151–160.

DOWNEY, D. J., SIMKIN, P. A. & TAGGART, R. (1988). The effect of compressive loading on intraosseous pressure in the femoral head *in vitro*. *Journal of Bone and Joint Surgery* **70A**, 871–877.

FAZZALARI, N. L., DARRACOTT, J. & VERNON-ROBERTS, B. (1983). A quantitative description of selected stress regions of cancellous bone in the head of the femur using automatic image analysis. *Metabolic Bone Disease and Related Research* **5**, 119–125.

FROST, H. M. (1964). *The Laws of Bone Structure*. Springfield, IL: Thomas.

MERTZ, W. A. & SCHENK, R. K. (1970). Quantitative structural analysis of human cancellous bone. *Acta anatomica* **75**, 54–66.

PARFITT, A. M., MATHEWS, C. H. E., VILLANEUVA, A. R., KLEEREKOPER, M., FRAME, B. & RAO, D. S. (1983). Relationships between surface, volume, and thickness of iliac trabecular bone in aging and in osteoporosis. *Journal of Clinical Investigation* **72**, 1396–1409.

REVELL, P. A. (1983). Histomorphometry of bone. *Journal of Clinical Pathology* **36**, 1323–1331.

SCHWARTZ, M. P. & RECKER, R. R. (1981). Comparison of surface density and volume of human iliac trabecular bone measured directly and by applied stereology. *Calcified Tissue International* **33**, 561–565.

SIMKIN, P. A. & DOWNEY, D. J. (1987). Hypothesis: Retrograde embolization of marrow fat may cause osteonecrosis. *Journal of Rheumatology* **14**, 870–872.

SIMKIN, P. A., GRANEY, D. O. & FIECHTNER, J. J. (1980). Roman arches, human joints, and disease. Differences between convex and concave sides of joints. *Arthritis and Rheumatism* **23**, 1308–1311.

SIMKIN, P. A., HOUGLUM, S. J. & PICKERELL, C. C. (1985). Compliance and viscoelasticity of canine shoulders loaded *in vitro*. *Journal of Biomechanics* **18**, 735–743.

SIMKIN, P. A., PICKERELL, C. C. & WALLIS, W. J. (1985). Hydraulic resistance in bones of the canine shoulder. *Journal of Biomechanics* **18**, 657–663.

WHITEHOUSE, W. J. (1974). The quantitative morphology of anisotropic trabecular bone. *Journal of Microscopy* **101**, 153–168.

WHITEHOUSE, W. J. (1980). Irregularities and asymmetries in trabecular bone in the innominate and elsewhere. *Metabolic Bone Disease and Related Research* **2S**, 271–278.

WHITEHOUSE, W. J., DYSON, E. D. & JACKSON, C. K. (1971). The scanning electron microscope in studies of trabecular bone from a human vertebral body. *Journal of Anatomy* **108**, 481–496.

WOLFF, J. U. (1870). Ueber die innere Architectur der Knochen und ihre Bedeutung für die Frage vom Knochenwachsthum. *Archiv für pathologische Anatomie und Physiologie und für klinische Medizin* **50**, 389–450.